Thermal conductance and the Peltier coefficient of carbon nanotubes

M. F. Lin and D. S. Chuu
Electrophysics Department, National Chiao Tung University, Hsinchu 30050, Taiwan, Republic of China

K. W.-K. Shung
Physics Department, National Tsing Hua University, Hsinchu 30043, Taiwan, Republic of China

(Received 11 September 1995; revised manuscript received 27 November 1995)

The π-band structure of one-dimensional carbon nanotubes is very special. Their ballistic transport properties are studied theoretically and are found to exhibit rich magnetic-flux-dependent structures. The thermal conductance $\kappa(\phi)$ has many step structures caused by the Zeeman splitting; a similar effect has been found in the electrical conductance $G(\phi)$. The Peltier coefficient $\Pi(\phi)$ vanishes in the zero-voltage limit at any magnetic flux due to the symmetric π-band structure about the chemical potential $\mu=0$. However, a finite Peltier effect could be observed by applying a finite voltage or by doping carbon nanotubes. Doping also causes peak structures with quantized maxima in $\Pi(\phi)$, as well as more step structures in $\kappa(\phi)$. Both the quantized peaks and the steps should be observable at $T<1$ K. These structures and also the validity of Wiedemann-Franz law $\kappa(\phi)\approx\pi^2k_B^2TG(\phi)/3e^2$ are found to depend upon the temperature, the chemical potential, the π-band property, and the Zeeman effect.

I. INTRODUCTION

The cylindrically coaxial carbon nanotubes recently reported by Iijima[1] have radii between 10 and 150 Å. This class of one-dimensional (1D) system has stirred a lot of recent studies.[2–20] One of the important advancements in experiments is that the single-shell carbon nanotubes could be produced in large-scale synthesis and their radii cover a wide range from 3.5 to 30 Å.[2,3] A single-shell carbon nanotube is predicted to be either a metal or a semiconductor,[4–8] depending on its radius and chirality. Furthermore, it could change drastically from being a metal (semiconductor) to a semiconductor (metal) as the magnetic flux ϕ (Ref. 7) through the nanotubes varies. The transport properties directly reflect the band property near the Fermi level. Hence transport measurements on a carbon nanotube could be used to test the validity of predicted band properties. The electrical conductance of a carbon nanotube has been studied theoretically within the ballistic regime.[11,12] In this work we further investigate the thermal and thermoelectric properties by evaluating the thermal conductance κ and the Peltier coefficient Π as a function of ϕ. The effects due to the Zeeman splitting, temperature, bias voltage, and doping are included in the study.

There are some transport measurements[13–15] on carbon nanotubes in the bundle form. These measurements show that such a three-dimensional (3D) bundle structure exhibits different transport properties. For example, the temperature-dependent resistivity varies logarithmically at lower temperature,[13] drops off quickly at higher temperature,[13,14] and exhibits a strong anisotropy between the parallel and perpendicular directions with respect to the tubular axis.[15] It is difficult to identify the π-band properties or to examine the theoretical predictions[4–8] from these measurements because the measured nanotube bundles are made up of different single-shell and multishell nanotubes. On the theoretical side, the electron-phonon scattering[16] is evaluated to estimate the electrical conductivity of carbon nanotubes and the electron-impurity scattering[17] could explain, qualitatively, the logarithmic temperature dependence in resistivity.

In this work, we mainly study the electric and thermal currents through a single-shell carbon nanotube within the ballistic regime. In low-dimensional systems, the ballistic electrical conductance exhibits the quantized step structures, which were studied by Landauer.[21] Streda[22] further predicted the quantized nature of thermoelectric properties such as in thermopower S. On the experimental side, the quantized transport properties in electrical conductance G,[23,24] thermopower,[25] Peltier coefficient Π,[26] and thermal conductance κ (Ref. 26) have all been identified in many systems. Carbon nanotubes, being a 1D system, should also exhibit these quantization phenomena.[12] Such behaviors are basically caused by the heat- and current-carrying subbands close to the Fermi level $E_F=0$. The carbon nanotube considered here is, in the presence of a uniform magnetic field B, along the tubular axis. The interaction[12,18,19] between the spin and the B field is taken into account so that the subbands could cross and intersect the Fermi level within a certain magnetic-flux range.[12,19] As a result, the ϕ-dependent thermal conductance exhibits step structures. Our calculations are performed at various temperatures so that we can find out under which conditions the step structures are observable and the approximated Wiedemann-Franz (WF) law $\kappa(\phi)\approx\pi^2k_B^2TG(\phi)/3e^2$ is valid. Since the conduction bands are symmetric, about $E_F=0$, to the valence bands, the ϕ-dependent Peltier coefficient and thermopower are found to vanish at any magnetic flux in the zero-voltage limit. Therefore, a finite bias voltage[27] is needed in study of the Peltier effect.

Doping could also induce quantized structures in $\kappa(\phi)$ and $\Pi(\phi)$. The alkali-metal atoms K and Rb (Ref. 20) have been successfully intercalated into carbon nanotubes, as done for graphite intercalation compounds[28] (GIC's) and carbon fibers.[29] Electrons in these cases are transferred from the intercalants to the carbon nanotubes; the Fermi energy thus

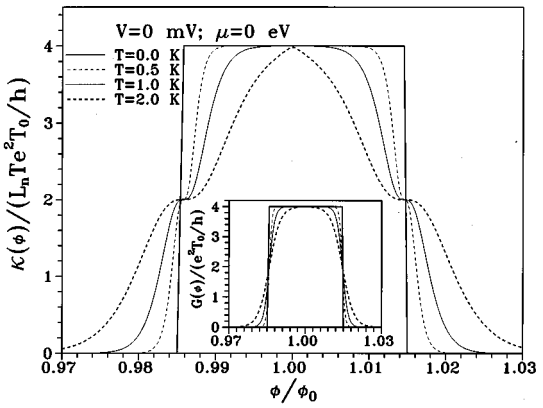

FIG. 1. Thermal conductance $\kappa(\phi)/(L_n T e^2 T_0/h)$ of the (210,0) nanotube at $V=0$ mV and $\mu=0$ eV, calculated at various temperatures. The electrical conductance is also shown in the inset for comparison.

increases from zero to a finite value.[8,19] There are many heat- and current-carrying 1D subbands intersecting with the Fermi level. When the Fermi level crossing takes place, $\kappa(\phi)$ and $\Pi(\phi)$ are expected to exhibit, respectively, a step structure and a peak structure with a quantized maximum.[22,30,31] Doped carbon nanotubes are found to display richer quantized structures as the magnetic flux varies, which suggests that the experimental verification of the ballistic behavior may be easier after doping.

This paper is organized as follows. The ballistic transport of a carbon nanotube in the presence of a uniform B field is discussed in Sec. II. The thermal conductance and the Peltier coefficient are calculated in Sec. III. Here the effects due to Zeeman splitting, temperature, bias voltage, and doping are also discussed. Finally, concluding remarks are presented in Sec. IV.

II. BALLISTIC TRANSPORT IN A UNIFORM B FIELD

The geometric structure of a carbon nanotube could be regarded as a rolled-up graphite sheet in the cylindrical form (Fig. 1 in Ref. 12). A carbon nanotube may be uniquely characterized by using a 2D lattice vector $\mathbf{R}_x=m\mathbf{a}_1+n\mathbf{a}_2$, where $\mathbf{a}_1$ and $\mathbf{a}_2$ are primitive lattice vectors of a graphite sheet. A carbon nanotube represented by (m,n) has a chiral angle $\theta=\tan^{-1}[-\sqrt{3}n/(2m+n)]$ and a radius $r=|\mathbf{R}_x|/2\pi=b\sqrt{3(m^2+mn+n^2)}/2\pi$. $b=1.42$ Å is the nearest-neighbor distance. It is sufficient to take a zigzag nanotube denoted by $(m,0)$, with $\theta=0°$, as a model study in understanding the essential characteristics of transport properties.

The $(m,0)$ nanotube here exists in a uniform B field parallel to the tubular axis ($\|\mathbf{e}_y$). The π-band structure is calculated within the tight-binding model like the one employed for a graphite sheet.[32] The energy dispersion is given by[6,12]

$$E(J,k_y,\sigma,\phi)=E(J,k_y,\phi)+E(\sigma,\phi), \tag{1a}$$

where

$$E(J,k_y,\phi)=\pm\gamma_0\left\{1+4\cos\left(\frac{3bk_y}{2}\right)\cos\left[\frac{\pi}{m}\left(J+\frac{\phi}{\phi_0}\right)\right]+4\cos^2\left[\frac{\pi}{m}\left(J+\frac{\phi}{\phi_0}\right)\right]\right\}^{1/2}, \tag{1b}$$

with the resonance integral $\gamma_0=3.033$ eV (Ref. 6) and

$$E(\sigma,\phi)=\frac{g\sigma}{m^*r^2}\frac{\phi}{\phi_0}. \tag{1c}$$

The only effect of the B field is to change the angular momentum (the subband index) from J ($J=1,2,\ldots,2m$) to $J+\phi/\phi_0$. The axial wave vector $|k_y|\leq\pi/3b$ is confined within the first Brillouin zone. The spin-B interaction $E(\sigma,\phi)=(g\sigma/m^*r^2)(\phi/\phi_0)$, where the g factor is the same as that ($\simeq 2$) of the pure graphite or GIC's,[28] $\sigma=\pm\frac{1}{2}$ is the electron spin, and m^* is the bare electron mass. When $E(\sigma,\phi)$ is neglected, a $(m,0)$ nanotube with $m=3\mathscr{I}$ ($\neq 3\mathscr{I}$) is metallic[7,12] at $\phi_a=\mathscr{I}\phi_0$ [$(\mathscr{I}\pm\frac{1}{3})\phi_0$], where $\mathscr{I}$ denotes an integer; it is semiconducting at other ϕ's. Under these conditions (i.e., $\phi=\phi_a$), $E_F=0$ touches both the conduction and the valence bands but only at the band edges. However, the spin-B interaction could cause the subbands to cross the Fermi level in the neighborhood of ϕ_a,[12,19] and its magnitude is estimated to be much larger than the energy gap due to the mixing effect[6] of the π and σ bands and the Peierls distortion.[6,7] Hence, with the Zeeman effect taken into consideration, a carbon nanotube is metallic within a certain magnetic-flux range near ϕ_a. This feature leads to step structures in the ballistic thermal conductance. The π-band structure [Eqs. (1a)–(1c)], where the conduction and the valence bands are symmetric about $E_F=0$, on the other hand, results in a vanishing Peltier coefficient $\Pi(\phi)=0$ at zero bias voltage.

The system under consideration is a single-shell zigzag nanotube threaded by a magnetic flux ϕ and suspended between two macroscopic leads (energy and particle reservoirs). When the bias voltage V and the temperature difference ΔT are applied between the two reservoirs, the electric and the thermal currents will flow through the carbon nanotube. The left and the right reservoirs are assumed to have the chemical potentials and the temperatures $(\mu+eV,T)$ and $(\mu,T+\Delta T)$, respectively, at which the electrons obey the Fermi-Dirac statistics. The chemical potential here needs to satisfy the condition[27,11] $eV+\mu\geq E_F\geq\mu$, where E_F is the Fermi energy of the carbon nanotube. $\mu=E_F$ is taken in the calculations even in cases when $V\neq 0$.[12] In the ballistic regime, the length of the nanotube needs to be shorter than the elastic and the inelastic mean free path, i.e., there should be no scattering inside the nanotube. The ballistic quantization effects are important only at $T<2$ K (see later). The inelastic mean free path at such a low-temperature range is estimated to be larger than 1 μm.[16] A nanotube of this length, made essentially impurity free, should be suitable for ballistic transport measurements. Furthermore, inelastic scattering is assumed to occur only in the reservoirs, and strong elastic scattering at the contacts between the carbon nanotube and the leads. After detailed derivations,[33] the net electric and thermal currents are, respectively, given by

$$I(\phi)=eT_0\sum_{J,\sigma}\int_{k_y>0}\frac{dk_y}{2\pi}\frac{1}{\hbar}\left|\frac{\partial E}{\partial k_y}\right|\left\{f^0\left(\frac{E-\mu-eV}{T}\right)-f^0\left(\frac{E-\mu}{T+\Delta T}\right)\right\} \tag{2a}$$

and

$$U(\phi)=T_0\sum_{J,\sigma}\int_{k_y>0}\frac{dk_y}{2\pi}\frac{1}{\hbar}\left|\frac{\partial E}{\partial k_y}\right|(E-\mu)\left\{f^0\left(\frac{E-\mu-eV}{T}\right)-f^0\left(\frac{E-\mu}{T+\Delta T}\right)\right\}, \tag{2b}$$

where $E=E(J,k_y,\sigma,\phi)$ [Eq. (1a)]. $(1/\hbar)\left|\partial E/\partial k_y\right|$ is the longitudinal velocity, T_0 [see Eq. (4) in Ref. 33] the net probability for electrons in the reservoirs to enter a carbon nanotube with the above velocity, and f^0 the Fermi-Dirac distribution function for electrons deep inside the reservoirs. $T_0=1$ in the absence of scattering at contacts.

When there is no temperature difference between two reservoirs, the Peltier coefficient is defined as[34]

$$\Pi(\phi)=\left.\frac{U(\phi)}{I(\phi)}\right|_{\Delta T=0} \tag{3}$$

in the vanishing bias voltage ($V\to 0$) limit. With $\mu=0$, the thermal current from the left reservoir is equal to that from the right reservoir [see Eqs. (2b) and (4b)], owing to the symmetry of the π bands about $\mu=0$. The net thermal current through an undoped carbon nanotube thus vanishes at any magnetic flux, and so does the Peltier coefficient. We note that the net electric current[12] through an undoped carbon nanotube does not necessarily vanish as $V\to 0$. A nonzero Peltier effect following Eq. (3), however, may be obtained at a finite voltage[11,12,27] (Fig. 3), where both the thermal and the electric currents are finite. The effect is then a nonlinear one. It should be noticed that doping leads to nonzero μ about which the conduction and the valence bands need not be symmetric and one can thus find nonvanishing $\Pi(\phi)$ for doped nanotubes as $V\to 0$ (see Fig. 5 later). On the other hand, at $\Delta T\neq 0$, the net thermal current must accompany the net electric current through a carbon nanotube.

Within the linear response ($\Delta T\to 0$ and $V\to 0$), $I(\phi)$ and $U(\phi)$ in Eqs. (2a) and (2b) are reduced to

$$I(\phi)=K_0(\phi)V-\frac{K_1(\phi)}{T}\Delta T \tag{4a}$$

and

$$U(\phi)=K_1(\phi)V-\frac{K_2(\phi)}{T}\Delta T, \tag{4b}$$

where

$$K_\alpha(\phi)=\frac{e^{2-\alpha}T_0}{h}\sum_{J,\sigma}\int_{k_y>0}dk_y\left|\frac{\partial E}{\partial k_y}\right|(E-\mu)^\alpha\frac{-\partial f^0(E)}{\partial E}. \tag{4c}$$

At low temperatures, the main contributions to K_α ($\alpha=1,2,3$) are from states very close to the chemical potential. When $\alpha=0$ is even (odd), the integrand in Eq. (4c) is a symmetric (antisymmetric) function about $E-\mu$. This explains why $\Pi(\phi)$ vanishes for undoped nanotubes in the $V\to 0$ limit. Moreover, at the same temperature, the integrand of $K_2(\phi)$, being quadratic in $E-\mu$, is more extended in energy than that of $K_0(\phi)$. Its consequences will be discussed later. At $\Delta T=0$, the electrical conductance $G(\phi)=I(\phi)/V=K_0(\phi)$ and the Peltier coefficient $\Pi(\phi)=K_1(\phi)/K_0(\phi)$.

The thermopower, which is the bias voltage developed by the system in response to a temperature gradient when $I(\phi)=0$, is given by

$$S(\phi)=\left.\frac{V(\phi)}{\Delta T}\right|_{I(\phi)=0}=\frac{K_1(\phi)}{TK_0(\phi)}=\frac{\Pi(\phi)}{T}. \tag{5}$$

This relation between the thermopower and the Peltier coefficient is the so-called Kelvin-Onsager relation. It is thus sufficient to study one of the two properties within the linear response. The thermal conductance, which is the net thermal current produced by a temperature gradient at $I(\phi)=0$, is given by

$$\kappa(\phi)=\left.\frac{-U(\phi)}{\Delta T}\right|_{I(\phi)=0}=\frac{K_2(\phi)-K_1^2(\phi)K_0^{-1}(\phi)}{T}\approx\frac{K_2(\phi)}{T}. \tag{6}$$

The term K_1^2/TK_0 ($\sim 10^{-5}K_2/T$) is very small for a carbon nanotube and is thus neglected in the following calculations, where Eq. (6) is employed for the calculations of the thermal conductance and Eq. (3) for the Peltier coefficient.

III. THERMAL CONDUCTANCE AND PELTIER COEFFICIENT

We choose the zigzag (210,0) nanotube as a model study. The radius of such a nanotube is ~ 80 Å, which is larger than the present-day available single-shell nanotubes. The quantized ballistic properties that we discuss here, however, are found to essentially depend on how 1D subbands cross E_F as the magnetic flux through the nanotubes varies; sizes of the nanotubes only affect when and where the crossing takes place. In other words, the results we obtain are general and may be applied to nanotubes of other radii. Moreover, the discussion here may be applicable to multishell nanotubes that have radii up to 150 Å. Intertube interactions in a multishell structure could modify the bands near E_F,[9,10] but would not destroy their 1D character; therefore our main results would remain valid in such a system. The same conclusion may not be applied to nanotube bundles. The intertube interaction in this case leads to a band dispersion in the perpendicular direction.[10] This destroys the 1D character, which is of central importance here. In short, our calculation shows that 1D ballistic properties should be observable in all single- or multishell nanotubes with radii up to 80 Å, but not in nanotube bundles.

At low temperatures, the thermal excitations are relevant only around ϕ_a (here $\mathcal{T}\phi_0$), where the carbon nanotube is either a metal or a semiconductor with a very small energy gap. The thermal conductance $\kappa(\phi)/(L_nTe^2T_0/h)$ (Lorenz number $L_n=\pi^2k_B^2/3e^2$) of the pure (210,0) nanotube is

shown in Fig. 1 around ϕ_0 at various T's. At $T\to 0$, there is a step structure (the heavy solid curve) for $0.9858\,\phi_0 \leqslant \phi \leqslant 1.0145\,\phi_0$, which is similar to the structure found in the electrical conductance[12] (inset). At a very low temperature,

$$K_2(\phi) \approx \frac{\pi^2 k_B^2 T^2 T_0}{3h} \sum_{J_a,\sigma} \approx \frac{\pi^2 k_B^2 T^2}{3e^2} K_0(\phi) \tag{7a}$$

and then

$$\frac{\kappa(\phi)}{L_n T e^2 T_0/h} \approx \sum_{J_a,\sigma} \approx \frac{G(\phi)}{e^2 T_0/h}. \tag{7b}$$

We have used the relation $\int_{-\infty}^{\infty} E^2 \,\mathrm{sech}^2(E/2)(dE/4) = \pi^2/3$ for $K_2(\phi)$ in Eq. (4c). The similarity between the thermal conductance and the electrical conductance is described by the approximated WF law [Eq. (7b)]. $\Sigma_{J_a,\sigma}$ in Eqs. (7a) and (7b) sums over the subbands either touching or intersecting the chemical potential ($\mu = 0$) and is proportional to the low-temperature thermal conductance. There are four heat-carrying subbands intersecting with $\mu = 0$, so the step structure has a height of 4. The four subbands include two spin-down conduction bands and two spin-up valence bands, with $J_a = 139$ and 279.[12] The conductance threshold at $\phi_c = 0.9858\,\phi_0$ ($1.0145\,\phi_0$) corresponds to the beginning (end) of the subband crossing of $\mu = 0$. The approximate ϕ_c was given in Eq. (10) of Ref. 19. Here the step structure in the thermal conductance is purely caused by the spin-B interaction. If there is no Zeeman splitting, the thermal conductance only displays step structures with vanishing widths at $\phi = \phi_a$. The characteristics (i.e., the position, the height, and the width) of the step structures are the same as those of the electrical conductance.[12] A similar conclusion may thus be drawn that the thermal conductance of the (m,n) carbon nanotube exhibits step structures with a height of 4 (2) in the neighborhood of $\phi_a = 3\mathscr{I}$ $[(\mathscr{I} \pm \frac{1}{3})\phi_0]$, when $2m+n = 3\mathscr{I}$ $(\neq 3\mathscr{I})$.

The step structure around ϕ_0 decreases quickly as the temperature increases from zero. The quantized structure is expected to be observable at $T \leqslant 1$ K. Furthermore, the thermal broadening effect is more important in the thermal conductance than in the electrical conductance. For example, the step structures in thermal conductance are completely lost at $T \leqslant 2$ K (the heavy dashed curve), while the similar structures in electrical conductance become indistinguishable at $T \geqslant 10$ K.[12] We reiterate here that although only a single-shell nanotube is considered here, a multishell system is expected to exhibit similar characteristics, only with more step structures at low temperatures,[12] and hence could be more easily identified. Being able to do so should be very helpful in understanding the π-band property close to $\mu = 0$.

The validity of the approximated WF law $\kappa(\phi) \approx G(\phi) L_n T$ is examined. The ratio $G(\phi)L_nT/\kappa(\phi)$ is shown in Fig. 2 at various temperatures. At $T\to 0$, the ratio (the heavy solid curve) approaches 1 (0) inside (outside) the magnetic-flux range, which corresponds to the subband crossing of $\mu = 0$. The integrand of $K_2(\phi)$ [Eq. (4c)] is more extended in energy than that of $K_0(\phi)$; therefore, $\kappa(\phi)$ is more sensitive to the thermal broadening effect than $G(\phi)$ is. In other words, the WF ratio cannot maintain at the predicted value of 1 when $T \neq 0$. The deviation from the WF law increases with the temperature and is most noticeable near the conductance thresholds, i.e., at ϕ around $0.9858\,\phi_0$, $1.0145\,\phi_0$, and 0 (inset). In short, the approximated WF law is valid only at a very low temperature and at a magnetic flux that corresponds to subband crossing but is away from conductance threshold.

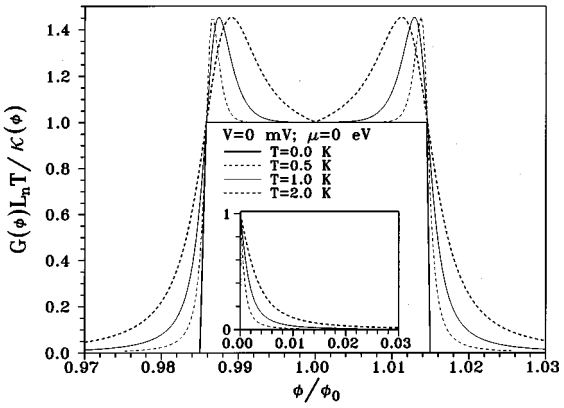

FIG. 2. Relation between the electrical conductance and the thermal conductance. $G(\phi)L_nT/\kappa(\phi)$ of the (210,0) nanotube at $V = 0$ mV and $\mu = 0$ eV, calculated at various temperatures. The inset shows the details at small ϕ's.

For a vanishing bias voltage, the antisymmetry of the integrand of $K_1(\phi)$ [Eq. (4c)] and the symmetry of the π band about $\mu = 0$ lead to vanishing thermal current and Peltier coefficient. However, there exists a nonzero electric current at ϕ that corresponds to the subband crossing of $\mu = 0$, and the electrical conductance exhibits the step structure there (e.g., inset in Fig. 1). On the other hand, a finite bias voltage V, as understood from the previous studies,[27,12] could broaden the step structure in $G(\phi)$. For example, such a quantized step is considerably broadened at $V > 1$ mV.[12] The broadening effect is mainly due to the elevation of the chemical potential in the left reservoir from 0 to eV. Such an elevation of chemical potential could also cause nonzero thermal currents and hence a finite Peltier coefficient following Eq. (3). $\Pi(\phi)$ at various bias voltages ($\geqslant 1$ mV) at $T = 0$ is shown in Fig. 3. $G(\phi)$ is also shown in the inset for

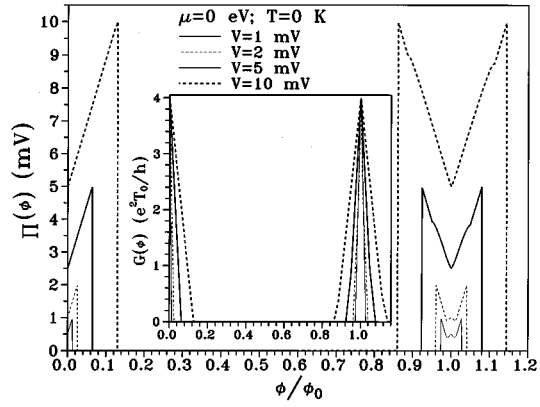

FIG. 3. Peltier coefficient of the (210,0) nanotube at $T = 0$ K and $\mu = 0$ eV, calculated at various bias voltages. The electrical conductance is also shown in the inset for comparison.

comparison. At $T=0$, both $I(\phi)$ and $U(\phi)$ have a factor $\theta(eV-E)-\theta(-E)$ [see Eq. (2)]. After the integration, one could find $I(0)\propto V$ and $U(0)\propto V^2$, i.e., there is a finite $G(0)$ but a vanishing $\Pi(0)$ as $V\rightarrow 0$. For $\phi\neq 0$, a finite band gap develops for the zigzag nanotube. When the energy eV is smaller than the energy difference E_D [Eq. (8)] between the conduction band and $\mu=0$, no states could carry thermal or electrical currents anymore. $\Pi(\phi)$ and $G(\phi)$, then, both vanish concurrently. For example, at $V=10$ mV, both $\Pi(\phi)=0$ and $G(\phi)=0$ (the heavy dashed curves) for $0.13\,\phi_0\leqslant\phi\leqslant 0.86\phi_0$.

For the (210,0) nanotube, E_D varies with ϕ and, from Eq. (1a), could be expressed as

$$E_D(\phi)=\frac{3b\gamma_0}{2r}\frac{\phi'}{\phi_0}-\left|\frac{g\sigma}{m^*r^2}\frac{\phi}{\phi_0}\right|, \tag{8}$$

where $\phi=\mathcal{J}\phi_0\pm\phi'$ and $\phi'\leqslant\phi_0/2$. $2E_D$ is the energy gap when $E_D\geqslant 0$. E_D increases, from zero, linearly in ϕ and reaches a maximum at $\phi_0/2$ before decreasing at the further increase of ϕ. E_D might become negative due to the subband crossing of $\mu=0$. Nonvanishing thermal and electric currents exist as long as $E_D(\phi)\leqslant eV$. A higher voltage could thus widen the window of passage and enhance $\Pi(\phi)$, and make the observation of the Peltier effect easier. Furthermore, $\Pi(\phi)$ may increase or decrease with the increasing ϕ, but in a way contrary to that displayed by $G(\phi)$. This feature relies on the way that the thermal and the electric currents vary with the magnetic flux. When, for example, $E_D(\phi)$ increases as ϕ varies, both $U(\phi)$ and $I(\phi)$ would decrease, but $U(\phi)$ would do so at a slower pace; therefore, while $\Pi(\phi)$ is increasing in value $G(\phi)$ is decreasing. In short, $\Pi(\phi)$ and $G(\phi)$ would vary in the opposite direction as ϕ varies. Also note that $G(\phi)$ (inset) has structures linear in ϕ for the simple reason that E_D varies linearly in ϕ.

Other than applying a finite voltage, the chemical potential may also be varied by doping. Here we assume that alkali-metal atoms[20] are intercalated into carbon nanotubes and that each carbon atom receives $0.1e$ on the average.[12,16] This is comparable to what has been found in the stage-one GIC's (C_8M, M=K, Rb, and Cs).[28,29] The doping is predicted to mainly cause the rigid shift[8] of the Fermi energy from zero to a finite value. According to the rigid-band model,[19] $E_F=2.1311$ eV for the (210,0) nanotube at this charge transfer rate. There are now free carriers in the conduction bands and they greatly enhance the thermal and the electric currents. Basic transport properties are also modified; for example, the Peltier coefficient and the thermal conductance both become quantized because of doping. Also note that the layered GIC's (Refs. 35 and 36) would not have the similar quantized transport properties of the 1D carbon nanotubes.

$\kappa(\phi)/(L_nTe^2T_0/h)$ of the doped (210,0) nanotube is shown in Fig. 4 at various T's and $V=0$ mV. At $T\rightarrow 0$, the thermal conductance [Eq. (7a)] is proportional to the number of subbands intersecting with the chemical potential ($\mu=2.1311$ eV). The lowering steps found at small ϕ are due to a decreasing number of subbands that cross μ as ϕ increases. This trend is reversed at larger ϕ. That $\kappa(0)=\kappa(\phi_0)$ follows from the fact that the band is periodic in ϕ if the spin-B interaction is neglected. At a different

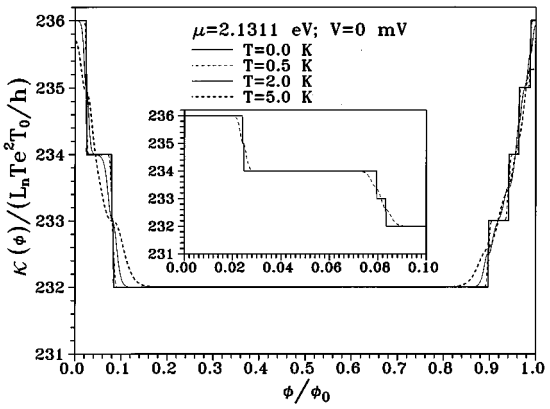

FIG. 4. Same plot as Fig. 1, but for the doped (210,0) nanotube with $\mu=2.1311$ eV. The inset shows the details at small ϕ's.

doping level we could find a different ϕ dependence in κ, but similar step structures would remain. The spin-B interaction, which leads to the Zeeman splitting, increases linearly with ϕ. Thus the splitting of a step into two halves due to the Zeeman effect becomes increasingly clear at larger ϕ's. A strong thermal broadening effect, as found in Fig. 1, could mask the step structures at $T>1$ K. Similar structures in $G(\phi)$ have been found and discussed in Ref. 12. We further discuss the relation between the thermal and electrical conductances, as shown in Fig. 2. For the doped (210,0) nanotube with $\mu=2.1311$ eV, the number of heat- and current-carrying conduction bands is at least 232, so that the ratio $G(\phi)L_nT/\kappa(\phi)$ is close to 1 (not shown). Due to the different sensitivity about temperature between $G(\phi)$ and $\kappa(\phi)$, the ratio would exhibit a strong fluctuation about 1 near subband crossing, just like in the undoped case. The fluctuation is stronger at higher temperatures. On the other hand, the approximated WF law is well obeyed in a wide range ($\phi\sim 0.2\phi_0$–$0.8\phi_0$) where there is no subband crossing; this is characteristically different from Fig. 2 of an undoped carbon nanotube. In short, the validity of WF law, besides its dependence on the temperature, the magnetic flux, and the band structure, also depends on the chemical potential in an important way.

The Peltier coefficient of the doped (210,0) nanotube is shown in Fig. 5 at various T's and $V=0$ mV. $\Pi(\phi)$ exhibits

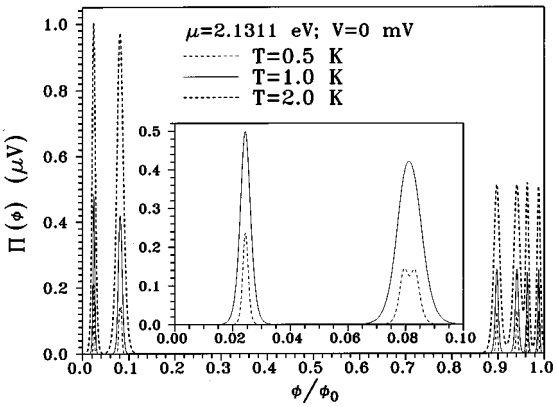

FIG. 5. Peltier coefficient of the doped (210,0) nanotube at $V=0$ mV and $\mu=2.1311$ eV, calculated at various temperatures. The inset shows the details at small ϕ's.

the oscillatory behavior and has several peak structures. These peak structures are related to the subband crossing of the chemical potential. As a conduction subband crosses the chemical potential, say at ϕ_c, the band structure in the energy range $\sim\mu\pm k_BT$ is very asymmetric about μ. Hence $K_1(\phi)$ of Eq. (4c) displays a local maximum at $\phi\doteq\phi_c$ and so does $\Pi(\phi)=K_1(\phi)/K_0(\phi)$. At very low temperatures, the Peltier coefficient is approximately given by[22]

$$\Pi(\phi=\phi_c)\approx\frac{k_BT\ \ln 2}{e\sum_{J_a,\sigma}}. \tag{9}$$

We have used the relation $\int_0^\infty E\ \mathrm{sech}^2(E/2)dE/4=\ln 2$ in evaluating $K_1(\phi_c)$. The variation of $\Sigma_{J_a,\sigma}$ with ϕ in Eq. (9) is negligible since there are many heat- and current-carrying conduction subbands. The quantized amplitude in the peaks of the Peltier coefficient is proportional to T, but that of the thermopower[22] is independent of T. For example, $\Pi(\phi)$ exhibits such a quantization phenomenon at ϕ close to ϕ_0. At $T<0.1$ K, $\Pi(\phi)$ is found to exhibit eight quantized peaks for $0\leqslant\phi\leqslant\phi_0$, which are centered at the magnetic flux corresponding to the subband crossing of μ. The quantized peaks are hardly affected by the thermal broadening at such a low temperature. But when the thermal energy k_BT is of the magnitude of the spin-B interaction, the thermal broadening could easily blur the quantized structures caused by the Zeeman splitting. For example, $\Pi(\phi)$ at $T=1$ K (the solid curve in the inset) does not exhibit the twin-peak structures at $\phi\sim 0.08\phi_0$. On the other hand, it would take a higher temperature ($T>10$ K) to completely destroy the quantized peaks related to the π-band structure. In general, the presence of the quantized peaks of $\Pi(\phi)$ relies on many factors, including the temperature,[30,31] the π-band structure, the spin-B interaction, and the chemical potential.

IV. CONCLUDING REMARKS

The electric and thermal currents through a carbon nanotube are studied within the ballistic regime. The magnetic flux could induce the subband crossing of the chemical potential. Therefore, the ballistic transport properties, the thermal conductance, the Peltier coefficient, and the electrical conductance[12] all exhibit rich magnetic-flux-dependent structures. For an undoped carbon nanotube with $\mu=0$, $\kappa(\phi)/(L_nTe^2T_0/h)$ exhibits step structures, but $\Pi(\phi)$ vanishes due to the symmetric π-band structure about $\mu=0$. However, the Peltier effect could be observed by applying a finite bias voltage or by intercalating with dopants into a carbon nanotube. In addition to inducing more step structures in the thermal conductance, doping also causes the peak structures with quantized maxima in the Peltier coefficient. Whether or not the approximated WF law is valid and the Peltier coefficient exhibits the quantized peaks depends on the temperature, the chemical potential, the π-band structure, and the spin-B interaction. The quantized peaks and steps should be observable at $T<1$ K. These quantized ballistic transport properties directly reflect the π-band structure of a carbon nanotube. The low-temperature measurements on carbon nanotubes are thus very important in revealing the π-band properties and also in testing the validity of the predicted π-band structure.[4–8] Effects of lattice vibrations[37] on the ballistic and the classical diffusive transport properties are worthy of further studies.

ACKNOWLEDGMENTS

This work was supported in part by the National Science Council of Taiwan, Republic of China under the Grants Nos. NSC-85-2112-M-009-020 and NSC-85-2112-M-007-027.

[1] S. Iijima, Nature **354**, 56 (1991).
[2] S. Iijima, P. M. Ajayan, and T. Ichihashi, Phys. Rev. Lett. **69**, 3100 (1992); S. Iijima and T. Ichihashi, Nature **363**, 603 (1993); P. M. Ajayan and S. Iijima, *ibid.* **361**, 333 (1993).
[3] C. H. Kiang, W. A. Goddard III, R. Beyers, J. R. Salem, and D. S. Bethune, J. Phys. Chem. **98**, 6612 (1994).
[4] J. W. Mintwire, B. I. Dunlap, and C. T. White, Phys. Rev. Lett. **68**, 631 (1992).
[5] N. Hamada, S. I. Sawada, and A. Oshiyama, Phys. Rev. Lett. **68**, 1579 (1992).
[6] R. Satio, M. Fujita, G. Dresselhaus, and M. S. Dresselhaus, Appl. Phys. Lett. **60**, 2204 (1992); Phys. Rev. B **46**, 1084 (1992); R. Saito, G. Dresselhaus, and M. S. Dresselhaus, *ibid.* **50**, 14 698 (1994).
[7] H. Ajiki and T. Ando, J. Phys. Soc. Jpn. **62**, 1255 (1993); **62**, 2470 (1993); N. A. Viet, H. Ajiki, and T. Ando, *ibid.* **63**, 3036 (1994).
[8] Y. Miyamoto, A. Rubio, X. Blase, M. L. Cohen, and S. G. Louie, Phys. Rev. Lett. **74**, 2993 (1995).
[9] R. Saito, G. Dresselhaus, and M. S. Dresselhaus, J. Appl. Phys. **73**, 494 (1993).
[10] Ph. Lambin, L. Philippe, J. C. Charlier, and J. P. Michenaud, Comput. Mater. Sci. **2**, 350 (1994); J. C. Charlier, X. Gonze, and J. P. Michenaud, Europhys. Lett. **29**, 43 (1995).
[11] W. Tian and S. Datta, Phys. Rev. B **49**, 5907 (1994).
[12] For details see M. F. Lin and K. W.-K. Shung, Phys. Rev. B **51**, 7592 (1995).
[13] X. N. Song, X. K. Wang, R. P. H. Chang, and J. B. Ketterson, Phys. Rev. Lett. **72**, 697 (1994).
[14] L. Langer, L. Stockman, J. P. Heremans, V. Bayot, C. H. Olk, C. V. Haesendonck, Y. Bruynseraede, and J.-P. Issi, J. Mater. Res. **9**, 927 (1994).
[15] W. A. de Heer, W. S. Bacsa, A. Chatelain, T. Gerfin, R. H. Baker, L. Forro, and D. Ugarte, Science **268**, 845 (1995).
[16] R. A. Jishi, M. S. Dresselhauss, and G. Dresselhauss, Phys. Rev. B **48**, 11 385 (1993); R. A. Jishi and M. S. Dresselhauss, *ibid.* **45**, 11 305 (1992).
[17] Z. Wang, M. Luo, D. Yan, H. Ying, and W. Li, Phys. Rev. B **51**, 13 833 (1995).
[18] P. J. Lin-Chung and A. K. Rajagopal, Phys. Rev. B **49**, 8454 (1994).
[19] M. F. Lin and K. W.-K. Shung, Phys. Rev. B **52**, 8423 (1995); **48**, 5567 (1993).
[20] O. Zou, R. M. Fleming, D. W. Murphy, C. H. Chen, R. C. Had-

don, A. P. Ramirez, and S. H. Glarum, Science **263**, 1744 (1994).
[21] R. Landauer, IBM J. Res. Dev. **1**, 223 (1957); Philos. Mag. **21**, 863 (1970).
[22] P. Streda, J. Phys. Condens. Matter **1**, 1025 (1989).
[23] B. J. van Wees, H. van Houten, C. W. J. Beenakker, J. G. Williamson, L. P. Kouwenhoven, D. van der Marel, and C. T. Foxon, Phys. Rev. Lett. **60**, 848 (1988).
[24] D. A. Wharam, T. J. Thornton, R. Newbury, M. Pepper, H. Ahmed, J. E. F. Frost, D. G. Hasko, D. C. Peacock, D. A. Ritchie, and G. A. C. Jones, J. Phys. C **21**, L209 (1988).
[25] L. W. Molenkamp, H. van Houten, C. W. J. Beenakker, R. Eppenga, and C. T. Foxon, Phys. Rev. Lett. **65**, 1052 (1990).
[26] L. W. Molenkamp, Th. Gravier, H. van Houten, O. J. A. Buijk, M. A. A. Mabesoone, and C. T. Foxon, Phys. Rev. Lett. **68**, 3765 (1992).
[27] P. F. Bagwell and T. P. Orlando, Phys. Rev. B **40**, 1456 (1989).
[28] M. S. Dresselhauss and G. Dresselhauss, Adv. Phys. **30**, 139 (1981).
[29] M. S. Dresselhauss, *Intercalation in Layered Materials* (Plenum, New York, 1987).
[30] C. R. Proetto, Phys. Rev. B **44**, 9096 (1991); Solid State Commun. **80**, 909 (1991).
[31] Y. Okuyama and N. Tokuda, Phys. Rev. B **46**, 2610 (1992).
[32] P. R. Wallace, Phys. Rev. **71**, 622 (1947).
[33] E. N. Bogachek, M. Jonson, R. I. Shekhter, and T. Swahn, Phys. Rev. B **47**, 16 635 (1993); **50**, 18 341 (1994).
[34] J. M. Ziman, *Principles of the Theory of Solids* (Cambridge University Press, Cambridge, 1972).
[35] J.-P. Issi, J. Heremans, and M. S. Dresselhaus, Phys. Rev. B **27**, 1333 (1983).
[36] T. Enoki, N. Sakamoto, K. Nakazawa, K. Suzuki, K. Sugihara, and K. Kobayashi, Phys. Rev. B **47**, 10 662 (1993).
[37] V. L. Gurevich, V. B. Pevzner, and K. Hess, Phys. Rev. B **51**, 5219 (1995).